Front. Struct. Civ. Eng. 2018, 12(3): 382–400
https://doi.org/10.1007/s11709-017-0430-x

REVIEW

A critical review of preparation design and workability measurement of concrete material for largescale 3D printing

Guowei MA[a,b*], Li WANG[c]

[a] *College of Architecture and Civil Engineering, Beijing University of Technology, Beijing 100124, China*

[b] *School of Civil, Environmental and Mining Engineering, The University of Western Australia, Crawley, WA 6009, Australia*

[c] *School of Mechanics and Civil engineering, China University of Mining & Technology at Beijing, Beijing 100083, China*

[*] *Corresponding author. E-mail: guowei.ma@uwa.edu.au*

ABSTRACT In recent few years, significant improvement has been made in developing largescale 3D printers to accommodate the need of industrial-scale 3D printing. It is of great feasibility to construct structural components and buildings by means of 3D concrete printing. The major issues of this innovative technique focus on the preparation and optimization of concrete materials which possess favourable printable properties as well as the measurement and evaluation methods of their workability. This paper firstly introduces three largescale 3D printing systems that have been successfully applied in construction industry. It then summarizes the commonly used raw materials in concrete manufacturing. Critical factors that should be particularly controlled in material preparation are specified. Easy-extrusive, easy-flowing, well-buildable, proper setting time and low shrinkage are significant for concrete mixture to meet the critical requirements of a freeform construction process. Thereafter, measuring methods that can be employed to assess the fresh and hardened properties of concrete at early stages are suggested. Finally, a few of evaluation methods are presented which may offer certain assistance for optimizing material preparation. The objective of this work is to review current design methodologies and experimental measurement and evaluation methods for 3D printable concrete materials and promote its responsible use with largescale 3D printing technology.

KEYWORDS 3D printing, concrete material, printable property, workability measurement, construction automation

1 Introduction

Various 3D objects can be replicated by printers in a layer by layer process. In the printing process, a digital 3D model is firstly created by dedicated software, or by the scanning of an existing object. Then, an algorithm is applied to cut the digital model into 2D slices. Finally, a printer builds the object slice by slice according to the digital prototypes [1,2]. In recent years, 3D printing systems have been successfully applied to constructing largescale structures. In 1998, Berokh Khoshnevis [3] at the University of Southern California (USA) developed a largescale 3D printing process called "Contour Crafting", which later becomes an effective method to print real-life houses. In 2007, an Italian engineer Enrico Dini [4] invented a largescale powder based 3D printer, named D-shape. This printer is claimed to produce a material with similar properties to marble. In 2014, WinSun [5], a company in China, built ten houses in Shanghai using a gigantic 3D printer (150 m × 10 m × 6.6 m) within 24 hours. Each building (200 m^2 floor area) was entirely created by high-grade cement and glass fibre. After that, they built the highest 3D printed building, a five-story apartment and the world's first 3D printed villa (1100 m^2 floor area). In 2015, Andy Rudenko [6] built a castle using a largescale 3D printer. The used material is a mix of cement and sand. Structural components were printed separately and assembled to the building. In 2015, the world's advanced saving project (WASP) introduced a huge 3D printer, named BigDelta, which measures 12 m

Article history: Received Dec 19, 2016; Accepted Apr 17, 2017

tall, 6 m wide and uses less than 100 watts of power. BigDelta printed an adobe structure at the open-air construction site using eco-friendly material of clay, straw, dirt and water. An elevator was connected to the scaffolding of printer to deliver the relatively solid materials [7]. The largescale 3D printing is of high potential to satisfy the requirements of diversification, industrialization, and automation for engineered construction.

It is noteworthy that when 3D printing comes into the field of real life building, the major issue is the design and preparation of concrete material that is compatible with the 3D printer. A few of cementitious material for 3D printing have been explored for construction applications. Gibbons et al. [8] investigated the feasibility of using rapid-hardening Portland cement (RHPC) to produce structures by a powder-binding 3D printing system. Maier et al. [9] demonstrated that calcium aluminate cements (CAC) is of high feasibility to be applied in 3D printing structures with favourable fresh and hardening properties. Xia and Sanjayan [10] developed a type of environmental friendly material, slag-based geopolymer, which was comprised of slag, silicate-based activator and fine sand. The proposed geopolymer has been proven to possess sufficient deposit ability to replace commercially available material in powder-based 3D printers, and shows good dimensional accuracy when utilized to print structures. The method developed in their study is readily scalable to produce large structural components. Khoshnevis et al. [11] proposed a kind of cementitious composite that is comprised of plaster and clay-like materials and could be smoothly extruded by contour crafting system, achieving a high surface-finish and highest geometric accuracy. The physical properties and printable performance, such as fluidity, buildability, extrudability, etc., of concrete for 3D printing are strongly dependent on the composition and characteristics of its constituents both in its fresh and hardened states [12]. Nerella et al. [13] developed a potentially replaceable material for concrete 3D printing using 31.1% brick, 22.3% limestone, 18.2% aerated concrete, 3.7% light-weight concrete. Printed specimen has a 21-day compressive strength of 80.6 MPa, 9.85% higher than that being casted. Lim et al. [14] developed a high performance cementitious mixture for concrete printing. It comprises 54% sand, 36% reactive cementitious compounds and 10% water by mass. The water to binder ratio is approximate to 0.28. The compressive strengths of extruded samples are 20% less than the standard cast specimen. While the flexural strength of extruded samples are close to the standard cast specimen. Feng et al. [15] studied the mechanical behaviour of 3D printed structures using cementitious powder. The average compressive strength of printed cubic specimens ranges 7.23 to 16.8 MPa, not suitable for structural members. Gosselin et al. [16] presented a novel premix of high performance printing concrete paste, which is composed of 30–40 wt% Portland cement, 40–50 wt% crystalline silica, 10 wt% silica fume and 10 wt% limestone filler. However, reported results are far from enough to provide references to material preparation for 3D printing and there is still no universally accepted agreement on the material selection, design procedure, interaction among the adopted constituents and their combination influences on the printability of concrete mixtures.

In general, the design and preparation of concrete for 3D printing mainly focus on optimizing the compatibility and coordination of concrete with the printer. The printable concrete mixture shall keep favourable flowability, extrudability, buildability, enough strength and low shrinkage, etc. To meet these requirements, significantly increasing the amount of cement is a usually adopted practice. However, this will inevitably lead to shrinkage due to the heat rising of cement hydration. Partly replacing the cement with mineral powders are commonly used in concrete preparation due to their good cementitious properties and pozzolanic reaction, which bring many advantages, i.e., low hydration heat, lime consuming, forming hydration products, filling the pores and voids, therefore improving many physical and mechanical properties [17,18]. Incorporating the mineral admixtures such as fly ash, silica fume, blast furnace slag, limestone filler and nano-silica etc. improve the fresh and hardened properties of concrete mixtures [19,20]. The physical and mechanical behaviour of concrete materials depend on the type and dosage of mineral admixtures and chemical additives as well as their compatibility in the mixing and hardening process [21]. Another approach to optimize the concrete material for 3D printing is employing chemical additives, such as superplasticizer, accelerator and retarder etc. to improve the workability of concrete systems for demanding applications. The influence of these admixtures and additives is the subject of ongoing studies. The addition of superplasticizer in concrete increases its fluidity without affecting the mechanical strength [22,23]. Viscosity modifying agent has been demonstrated to be very effective in stabilizing the rheological properties and consistency of concrete and in enhancing its dimensional stability [24].

In addition to the determination of raw materials and chemical additives, another important issue is the measurement and evaluation of the fresh and hardening properties of concrete mixtures so that they can be designed to be printed in an optimal way and behave as designed. The most important parameter for the concrete for 3D printing is the setting time. Vicat needle test is a widely used method to test the setting behaviour. Unfortunately, it cannot continuously record the setting and hardening processes and does not have the ability to measure setting properties of quick-setting materials [25]. Lots of investigations have been made during the last few years to detect setting and hardening properties of concrete pastes with different ultrasonic methods, such as ultrasonic

wave reflection method and ultrasonic wave transmission method [26,27]. These two types of ultrasonic methods are significantly different in monitoring the setting process of mortar and concrete. Voigt's results [28] revealed that the wave velocity obtained from transmission method is consistent and direct related to reflection loss obtained from reflection method. Sharma et al. [29,30] proposed an ultrasonic guided wave monitoring technique which detects the propagation of ultrasonic waves in embedded steel reinforcing bars to monitor the hardening process of freshly poured concrete. This method is suitable to in-situ and largescale structures. Liu et al. [31] have demonstrated a reliable in-situ ultrasonic method that utilizes embedded piezo-ceramic bender elements to monitor the setting of mortars.

This paper conducts a comprehensive review on the preparation design and workability measurement of concrete materials for 3D printing. It is organized as follows. The first section of this paper gives an overview of the recent reported largescale 3D printing techniques. The paper then focuses on issues of material selection and preparation design of concrete material to accommodate the requirements for largescale printing techniques. Various measuring and evaluating method and devices in respect to testing the workability, passing ability, viscosity, setting time and stiffness development of early age concrete are then introduced. Finally, in the last section a few of concluding remarks are drawn.

2 Construction-scale 3D printing

3D printing is a process in which various materials (liquid, powder, solid or sheet material) are successively solidified layer upon layer by extrusion, sintering, binding, polymerizing or other printing technology, and finally accumulating to form solid models. Each layer is equivalent to a cross section of the digital model and they fuse together to create the final shape [32,33]. In recent years, the development of largescale additive manufacturing has been developed to accommodate the need of architecture and construction. D-Shape is a large 3D printer that selectively binds sand with magnesium-based binder in order to create stone-like objects [14]. Contour crafting (CC) is a mega-scale automatic construction process that can reliably print out very large objects with dimensions of several meters, which is contributed by equipping with a multi-axis robotic arm. It is proved to be the most effective method to approach high speed automated construction [34]. Similar to contour crafting, concrete printing is another largescale construction process. 3D concrete printing constructs objects and structures by continually depositing cement mortars, but this method has a smaller resolution of deposition, results in better controlling of complex geometries [16]. Fig. 1 presents some structures manufactured via largescale 3D printing.

3 Preparation of concrete material for 3D printing

As above section cited, it is of great feasibility to 3D print real-life structures and buildings. Most of all is the preparation of high performance cement-based materials that compatible with corresponding printers. Raw materials usually perform significant influences on the fresh and hardening properties of concrete material. Considering the concrete mixture should be easy-flowing and easy-extrudable, aggregate and coarse sand must be eliminated during the preparation. The concrete material for 3D printing shall mainly comprise of powder materials to meet the required printability. Meanwhile, the inclusion of certain amount of chemical additives in concrete can offer positive contributions to coordinate the fresh properties of concrete with the largescale printer.

3.1 Raw material selection

Incorporating mineral admixtures in printable concrete preparation is greatly recommended. The widely considered powder mixtures in concrete manufacturing include fly ash (FA), silica fume (SF), blast furnace slag (BFS),

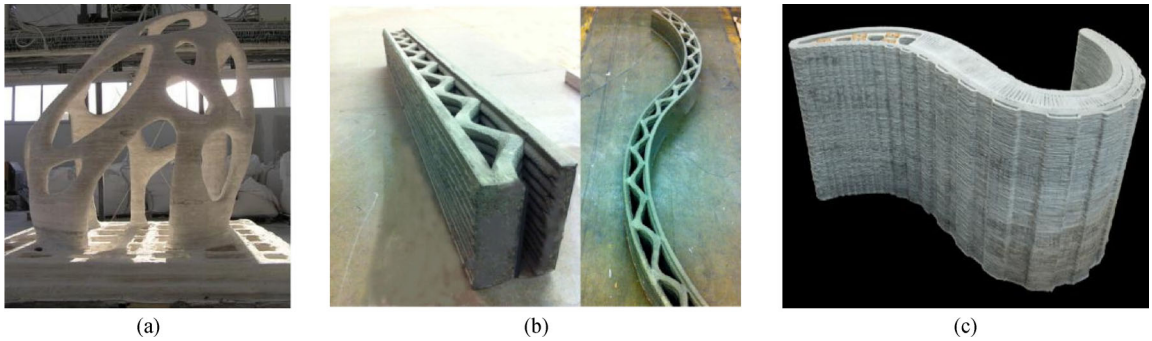

(a) (b) (c)

Fig. 1 Structures manufactured via 3D printing [14]. (a) 1.6 m high sculpture printed by D-shape; (b) hollow walls with corrugated internal structure printed by contour crafting; (c) wonder bench (2 m × 0.9 m × 0.8 m) produced by concrete printing

limestone filler (LF) and nano-silica (NS) as well as Portland cement (PC). Utilization of these materials provide significant technical benefits to concrete, including improved flowability, strength, durability performance, dimensional stability and lower heat of hydration. Table 1 lists the main chemical constitution and physical features of these powder materials. Except for NS, particle diameters of powder materials are in micrometre scale. Fig. 2 illustrates the physical characteristics of mineral mixtures and their applicability in different kind of concrete.

In general, proper addition of fine-grounded admixtures can improve the fluidity, stability and early stage strength of concrete due to their fine particles and high pozzolanic reactivity [35,36]. Meanwhile, admixtures could reduce the hydration heat caused by Portland cement, leading to better controlling of shrinkage. The replacement of cement with fine powders with different micro-shape, particle size distribution, packing density, surface area and zeta potential change will result in different workability of concrete paste [37].

(1) Silica fume

Silica fume (SF), also known as micro silica, is one of the most effective supplementary cementitious materials. It is a powder by-product produced in the smelting industry. The two major physical features of silica fume are its high content of amorphous SiO_2 and extreme fineness. SiO_2 content of SF varies from 61% to 98% based on the type of alloy being produced [39]. Silica fume consists of spherical particles with particle diameter around 0.1–0.5 μm and its Blaine fineness is in the range of 13,000–30,000 m^2/kg. Proper addition of SF contributes to the workability and strength improvement of concrete through pozzolanic reactions with free lime and void-filling effect [40,41].

(2) Fly ash

Fly ash is one of the main residues generated in combustion by-product from coal-fired power plants. There are two main types of fly ash, class F and class C. Class F fly ash is produced from burning anthracite or bituminous coal, which is low in CaO ($\leqslant$15%) and high in SiO_2 ($\geq$70%). Class C fly ash is produced from the burning of sub-bituminous coal and lignite, which is with higher CaO content (15%–30%). Elevated CaO gives class C fly ash unique self-hardening characteristics. Moreover, adding fly ash in concrete can densify the cement matrix by filling pores, leading to improvement of mechanical strength [42,43].

(3) Blast furnace slag

Ground granulated blast furnace slag is a kind of by-product obtained from the steel manufacturing industry. It can be used as a constituent for cement and a mineral admixture for making high performance concrete. Similar to most cementitious materials, it also possess high reactivity due to its ultra-fineness. The reactivity of blast furnace slag depends on the properties of slag, which vary with the source of slag, type of raw material used, method and the rate of cooling [44].

(4) Limestone filler

Limestone filler is a product obtained from the fine grinding of limestone. It is another notably used mineral admixture taken as cement replacement materials. It contains a high degree of calcium carbonate (Ca_2CO_3). Substitution of limestone fillers in concrete has grown due to it is actually cheaper and well-adapted and can present several advantages over ordinary cements. The diameter of limestone fillers ranges in the order of 7–120 μm. Utilization of limestone filter in concrete preparation can modify the packing density of cement grains and improve the workability of concrete mixtures [45,46].

(5) Nano-silica

Nano-silica (nano-SiO_2) has attracted considerable scientific interest in concrete technology due to its enhancing effect in workability, strength and durability [47]. Nano-powders have a remarkable surface area and nanoscale particles (Fig. 2). SEM studies reveal that the nanoparticles can densify the microstructure of cement paste by filling up the pores and further promote cement hydration due to the high pozzolanic activity, leading to considerably improve-

Table 1 Main chemical constitution and physical properties of cementitious materials

Chemical analysis	PC	FA	SF	BFS	LF	NC
CaO (%)	62.3–62.58	2.86–4.24	0.45	34.12–40.38	52.9–55.6	–
SiO_2 (%)	20.25–21.96	53.33–56.2	90.36–92.3	34.35–36.41	0.13–1.84	99.9
Al_2O_3 (%)	4.73–5.31	20.17–27.65	0.71	10.39–11.36	0.09–1.37	–
Fe_2O_3 (%)	3.68–4.04	6.04–6.69	1.31	0.48–0.69	0.24–0.47	–
Blaine fineness (m^2/g)	0.33–0.38	0.29–0.38	13–30	0.35–0.45	0.44–0.53	60–160
Specific gravity (g/cm^3)	3.15	2.08–2.25	2.22–2.33	2.79	2.58–2.65	–
Loss on ignition (%)	1.90–3.02	1.78–3.46	1.80–2.5	1.64	40.8–42.3	$\leqslant$1.00

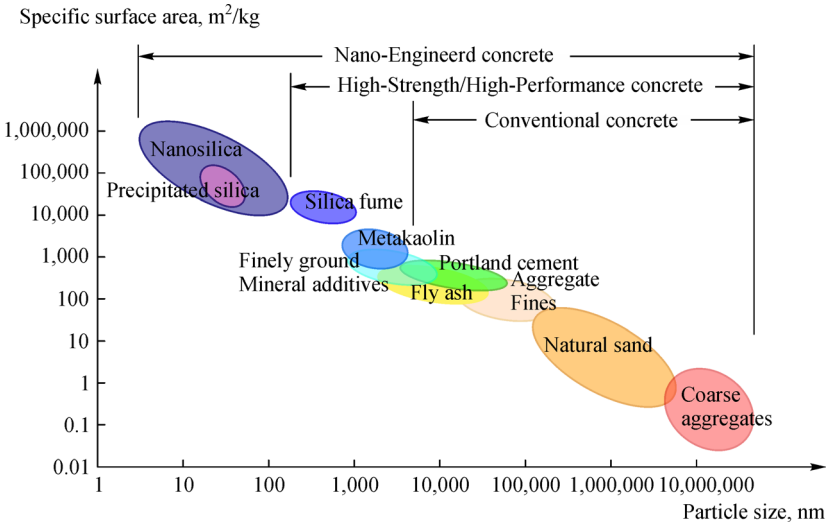

Fig. 2 Particle size and specific surface area related to concrete materials [38]

ment in mechanical strength [48,49]. However, nanoscale particle and ultra-high surface area of nano-SiO_2 increase the water requirement when it is adopted in preparing concrete, resulting in less flowability and more cohesive and viscous.

3.2 Chemical additives selection

(1) Superplasticizer

Superplasticizers are preferred in concrete preparation for their ability to reduce the water requirement while maintaining workability and enable the improvement of strength. Fig. 3 illustrates the working mechanism of superplasticizer. Cement particles are dispersed by repulsive force generated by negatively charged superplasticizers and the entrapped water would be released. Therefore, the flow characteristics of concrete are improved [50,51]. XRD and SEM analysis indicate that addition of superplasticizer does not alter the types of hydration products, but improves the degree of crystallinity and results in highly amorphous hydrates [52]. A variety of superplasticizers are developed available in the market. They are broadly classified into four basic groups, lignosulfonic acid (LS), melamine form-aldehyde sulfonic acid (SMF), naphthalene formaldehyde sulfonic acid (SNF) and polycarboxylic acid (CE) [53]. Table 2 presents the characteristics of usually used superplasticizers. Their influence on the flow characteristics, setting time and yield strength differs considerably even from the same group due to the different molecules structure and chemical configuration [54–56]. Chandra et al. [57] have studied the influence of superplasticizer type and dosage on the fluidity of cement mortars at different water to cement ratio. The results reveal that CE-based superplasticizer is most effective in fluidity improvement followed by LS, SNF and SMF.

(2) Accelerator

Concrete materials for 3D printing require a short setting time to promote the material to acquire enough early strength right after being deposited from nozzles. Setting accelerators are a class of admixtures commonly used for concrete to produce an immediate set. Accelerating agents includes chemical compositions that contribute to the

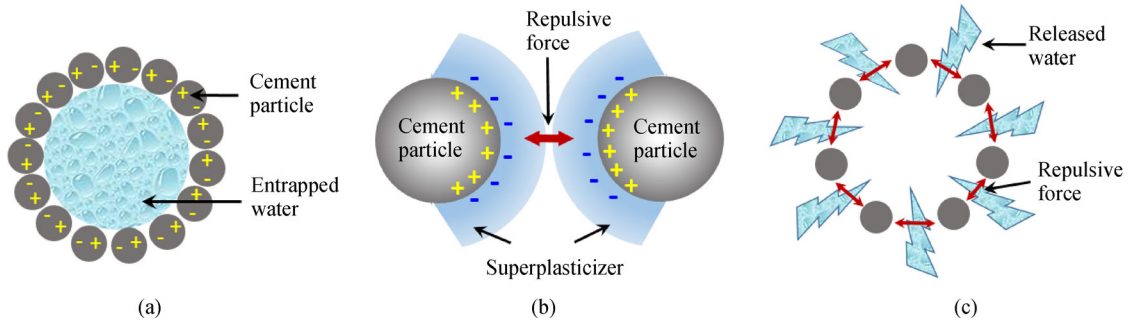

Fig. 3 Action of superplasticizer on cement particles. (a) Flocculated cement particles; (b) dispersing cement particles by repulsive force generated by negatively charged superplasticizer; (c) releasing of entrapped water

Table 2 Characteristics of usually used superplasticizers

Name	Solid content (%)	Density (g/cm^3)	Concentration (%)	Water reducing rate (%)	Suggested dosage (%)
SMF	33	1.13–1.18	20–35	15–30	0.5–1.5
SNF	> 95	1.09–1.20	> 40	12–20	1.5
LS	> 95	0.98–1.02	15–25	9–11	0.25
PCE	30–40	1.05–1.09	36–40	25	0.4– 1.2

quick development of cement hydration, thereby shortening the setting time and promote the speed of early stiffness development. The main classes of accelerating admixtures are either alkaline or alkali-free [58].

(3) Retarder

Retarder can be adsorbed on the surface of cement particles to form an insoluble layer, which delays the hydration of cement. Sodium gluconate (SG), tartaric acid (TA), citric acid (CA) are usually adopted retarders which perform favourable retarding effect [59,60].

(4) Viscosity modifying agent

Viscosity modifying agents (VMA) are water soluble polymers that control the flow characteristics and rheological performance of concrete mortars. Incorporating a small dose of viscosity modifying agent can reduce segmentation and enhance the dimensional stability of the concrete mortars. The VMA also brings down the powder requirement and still maintains the required stability [24]. The VMA polymer chains are connected one to the other by the Van der Waals interaction effect up to the blocking of the free water movement. This action leads to an increase in the mixture plastic viscosity. However, it is should be noted that if concrete is delivered in the 3D printer by pumping. Mortars with a higher viscosity may require a larger pumping pressure.

4 Printability optimization of concrete for 3D printing

4.1 Flowability control

Flowability is a key parameter to evaluate the printable performance of concrete mixture. Flowability controlling makes sure that the paste can be easy-pumpable in the delivery system and easy-depositable in the deposition system.

The particle grading of concrete paste is a main factor that governs its rheology and fluidity in the fresh state. Generally, a wider particle size distribution would contribute to a higher packing density and yield a better flowability [61,62]. Through proper mix proportioning, fine powder admixtures would densify the microstructures by filling the voids and pores and play a lubricating effect to prevent cement particle from bonding together, thereby enhancing the flowability of mortars [63,64]. Grzeszczyk and Lipowski [65] reported that the grinded fly ash promote the acquisition of better fluidity as compared with that coarse fly ash. However, incorporating excess content of fine powders may increase the inter particle friction and increase the viscosity of the paste, leading to negative effect to fluidity [66]. Mastali et al. [67] indicated that replacing cement with 14 wt% silica fume resulted in increasing slump flow time (T_{50}) about 40%. Guneyisi et al. [68] demonstrated that the T_{50} flow time and V-funnel flow time of SCC mixture manufactured with Portland cement replaced by 50% of fly ash is reduced by 43.2% and 15.6%, respectively.

In most cases, superplasticizers are preferred to improve the flowability of cement paste while maintaining comparable or higher mechanical strength to increasing water content. The addition of superplasticizer would disperse the flocculated cement particles, thereby releasing some of the water trapped inside the voids to increase the rheology fluidity of the paste [69,70]. Although a higher water to binding material ratio could lead to increase the flowability of concrete mixtures, it induces large pore or void content, reducing the mechanical strength to a large extent [71]. Leemann and Winnefeld [72] reported that adding VMA in cement pastes decreases the flowability at a constant water content, however, it can increase corresponding yield stress and plastic viscosity. Zhang et al. [60] studied two retarders, citric acid (CA) and sodium gluconate (SG), on the fluidity, flow loss and compressive strength of cement mortar. Their results show that the setting time continuously increased when the CA dosage increased. However, the initial fluidity was increased by CA at the dosage of 0.03 wt%, while decreased at the dosage of 0.06–0.15 wt%. SG performs similar effects. The optimum dosage of SG was suggested as 0.12 wt%. Li et al. [73] also investigated the influences of retarder CA and SG on the flowability of cement paste. Appropriate dosage of SG resulted in a better workability of cement pastes, however, CA does not. There was an apparent effect of competitive adsorption between CA and superplasticizer. Contrarily, the negative effect of SG was not remarkable. They suggested that the optimal dosages of SG should be controlled in the range of 0.03%–0.09% in order to ensure higher fluidity and lower flow loss for cement mortars.

4.2 Extrudability control

The cementitious materials for 3D printing need to have an acceptable degree of extrudability, which relates to the capacity of material to continuously be delivered through the small pipes and deposited form nozzles at the printing head.

Extrudability control of concrete material for 3D printing lies in a smooth grading of materials. Alternative raw materials should have rounded shape and fine particles. Compared to angular aggregates, employing round shape aggregates would enable a better control of extrudability and decrease blocking potential for a given water to powder ratio. Generally, basic principle of grading design for printing material is to use a considerable volume of cementitious paste to fill the voids formed between smooth graded aggregate particles [67,73]. A certain amount of trials have been carried out to explore the optimal extrudability control for concrete materials. Malaeb et al. [75] suggested a suitable mixture for 3D printing systems. The particle grading is strictly controlled. They recommended that the mass ratio of fine aggregate to cement is 1.28 and fine aggregate to sand is 2.0. And the maximum size of an aggregates is set as 1/10 of the diameter of the printing nozzle. Le et al. [76] selected sand with a maximum size of 2 mm to manufacture concrete paste used for a small nozzle with a diameter of 9 mm, which ensures a high printing resolution. The optimum binder mixture of a high-performance printing concrete was suggested to contain 70% cement, 20% fly ash and 10% silica fume by mass. And the sand to binder ratio was suggested by 3:2. Perrot et al. [12] prepared a kind of cement mortar used for 3D printing extrusion systems, which contains 50% cement, 25% limestone filler and 25% kaolin by mass. The average particle size of these three powders is 10 μm, 9 μm and 15 μm, respectively.

4.3 Buildability control

Buildability is another critical parameter to evaluate the printable performance of concrete materials, which refers to the ability of material to retain its extruded shape under self-weight and pressure from upper layers. Buildability can be considered as the early stage stiffness. The extruded cementitious paste must have enough buildability to guarantee it being lay down accurately, keep the form right after deposition, be hard enough to bear the weight of subsequent layers without collapsing and still be capable to binding adjacent layers.

In regular concrete material, aggregate constitutes a bulk of volumes, therefore providing favourable dimensional stability. In the case of printing cementitious paste, similarly, favourable buildability is achievable at relatively higher content of fine aggregate and sand. Tang et al. [77] have mentioned about the effect of fly ash on viscosity increase and proposed that fly ash can increase the energy demand in order to reach sufficient workability. From another perspective, chemical additives could offer positive contributions to the development of buildability. Incorporating a small doses of viscosity modifying agent (VMA) can reduce bleeding and improve the stability of the concrete mortars. The VMA also brings down the powder requirement and still maintains the required stability [24]. Benaicha et al. [78] indicated that addition of the VMA can make the 1-day compressive strength all self-compacting concrete above half of 28-days strength. This ratio demonstrates that VMA can present noticeable improvements at early age. Early strength agent could accelerate the hydration and rapidly shorten the setting time of cement. Therefore, the buildability of cement paste can be promoted. Lin et al. [59] have investigated the influence of three types of early strength agent, lithium carbonate, lithium hydroxide and sulfates, on the strength of cement-based printing material. Test results show that a ratio of 0.05% lithium hydroxide can shorten setting time to 9 min and cement mixed with lithium hydroxide indicates the highest improvement of 2-hour strength than the other two.

4.4 Setting time control

Printing material requires a long setting time to maintain a continuous flow and deposition process of the cement mortar. However, printable material still requires a short setting time to promote the material acquire enough early strength right after being deposited out from nozzles.

Robeyst et al. [79] measured the BFS replacement ratio to Portland cement on the setting property of concrete mixture. The results show that the stiffness development or setting process is generally retarded if more than 30% of the cement is replaced by BFS and the slower setting becomes clear at replacement levels of above 50%. Gesoglu et al. [80] proposed that binary use of BFS with ordinary PC significantly prolonged the initial and final setting times and reduced the viscosity of the concrete mixtures.

Setting property controlling of concrete primarily lies in the utilization accelerators and retarders. Paglia et al. [81] investigated the setting behaviour of cementitious mixture mixed with different type of accelerators. Results indicated that the setting time of concrete with 4.5% mass dosage of alkaline accelerators approximately was about 57% of that with 8.0% mass dosage of alkaline-free accelerators. The study results of Maltese et al. [82] showed a dosage of alkali-free accelerator from 2% to 7% by cement mass reduced the setting time of cement paste from 360 to 150 minutes. Galobardes et al. [83] recommended that the accelerator shall be directly added after the dry mixing process without dilution with water. The mixing time and mixing speed after accelerator addition was suggested for 20 s and 52 rpm, respectively. Lin et al. [59] tested the effect of six common retarders on the setting time of extrudable printing material. Among them, the optimal retarder for the cement-based paste was sodium tetraborate, the mix ratio of which from 0.1% to 0.3% could increase the jelling time from 28 to 109 minutes, and the final setting time from 49 to 148 minutes. Sodium gluconate and tartaric acid also performed favourable retarding effect.

4.5 Mechanical property control

Fine powder admixtures with smaller particle size than Portland cement tend to fill the voids and increase the packing density of cement matrix, resulting in higher stiffness and strength of concrete. Moreover, as illustrated in Fig. 4, enhancement of mechanical properties is also contributed by the high pozzolanic activity of silica fume and fly ash, which are rich in SiO_2. SF and FA reacts chemically with calcium hydroxide (C-H) formed during cement hydration and accelerate the formation of calcium silicate hydrates (C-S-H), therefore making the cementitious matrix denser and more compact and improving the mechanical strength of cement mortars. Gesoglu et al. [84] obtained that the use of silica fume on the strength development of concrete was very effective. Addition of 10% silica fume by mass increased the compressive strength by 8%–20% compared with the plain concrete. However, it is reported that the pozzolanic activity of silica fume at early ages is low. Its reaction with hydration products begins to occur after 3 days of hydration [85]. Benaicha et al. [78] reported that the compressive strength ratio (1 day/28 days) of concrete decreased with the increase of the silica fume content which ranges from 5% to 30%. This shows that silica fume is not contributed to stiffness gain at early stages. Li [86] showed that addition of 4 wt% of nono-SiO_2 increased the 3-day strength of high strength concrete by 81%. Ye et al. [87,88] reported that a small amount (3 wt%) of nano-SiO_2 could make cement paste thicker, accelerate the cement hydration process and enhance the early age compressive strength. Jo et al. [89] showed that the 7-days and 28-days compressive strengths of concrete paste with nano-SiO_2 particles were all higher than those containing silica fume. Meanwhile, nano-SiO_2 shows greater pozzolanic activity than silica fume. According to the findings of Guneyisi et al. [68], utilization of 4 wt% nano-silica increased the compressive strength of self-compacting concrete up 71.1%, while utilization of 6% decreased it. It was supposed that balling of nanoparticles may occurred when nano-silica used at 6% content. Therefore, dispersing agent is needed to ensure nanoparticles are effectively dispersed [38]. It is worthy noting that a large amount of fly ash adoption in concrete preparation will remarkably reduce its early stage strength [90]. But the initial pozzolanic activity of fly ash could be significantly improved after incorporating a little nano-SiO_2 [86]. However, according to the results reported by Liu et al. [91], fly ash has a slow initial pozzolanic reaction, which leads to later ages contribution to strength development. Ghazel and Khayat [92] proposed that substituting a large amount of cement by limestone powder decreased the cement requirement to achieve equivalent compressive strength at early ages.

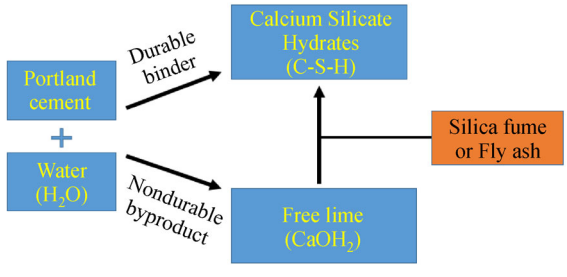

Fig. 4 Both silica fume and fly ash attribute to the mechanical strength development by reaction with free lime due to the high content of SiO_2

4.6 Shrinkage control

Shrinkage is an important concern that associates with the printing performance of cementitious material since it affects the dimensional accuracy and stability of printed structures. As discussed above, concrete material for 3D printing requires high water content to ensure good flowability and extrudability. As a result of this special requirement, excess water is added beyond the volume necessary for hydration. The excess water evaporates from the cement, leading to a high drying shrinkage deformation during setting and hardening process of the composite [93]. Moreover, 3D printed components always have larger area of surfaces directly exposed to ambient conditions than conventionally casted structures using mould or formworks. This case would promote the evaporation of free water [94].

Increase the content of mineral admixtures is one feasible solution to control the shrinkage. For a given age, a low value of W/C can reduce the drying shrinkage strain. The more the fine aggregate, the less the shrinkage deformation of the composite [95]. Employing fly ash in concrete mixture may significantly decrease the heat accumulation and reduce external cracking due to its lower release of hydration heat. Khatib et al. [96] investigated the influence of incorporating increasing amounts of fly ash in SCC. Tests results indicated that there was a linear reduction in shrinkage with the increasing content of fly ash. Replacing cement with 80% fly ash can reduce the shrinkage by 66.7%. Rongbin and Jian [97] demonstrated that shrinkage under drying condition decreases by over 80% by a combined use of fly ash and calcium sulfo-aluminate cement. In the studies of Guneyisi et al. [98], the drying shrinkage of concrete with 5% and 15% silica fume were approximately 29% and 35% less than the plain concrete. Al-Khaja [99] showed that adding silica fume in concrete could reduce the shrinkage strain by up to 34.9%. Jianyong and Yan [100] have also concluded that ultrafine ground granulated blast furnace slag and silica fume can substantially reduce the

shrinkage strain by accelerating the hydration process, which promotes the formation of stronger and denser microstructures and higher resistance to applied forces. It can be used to explain the enhancing effect of ultrafine mineral admixtures on drying shrinkage control of concrete. However, some researcher demonstrated that increasing silica fume content increased the autogenous shrinkage. Mazloom et al. [101] concluded that addition of 10% and 15% silica fume increased the autogenous shrinkage of concrete by 33% and 50%, respectively. In general, effects of silica fume on drying shrinkage are mainly governed by two balancing factors: 1) the shrinkage stress caused by capillary tension in the pores which promoted the shrinkage and 2) rigidity or stiffness development due to the densified matrix which restricted the shrinkage [39,102].

Adoption of chemical additives is an alternative method to prevent shrinkage. Shah et al. [103] showed that a significant decrease of the shrinkage could be obtained using shrinkage reducing admixture (SRA) in concretes. SRA is helpful in lowering the surface tension induced by water evaporation from the outer part of concrete.

5 Workability measurement of concrete for 3D printing

The fluid characteristics, setting behaviours, viscosity performance are critical features which can specify the printability and stability of concrete for 3D printing. Each behaviour can be detected by one or more experimental methods. The concrete material for 3D printing shall stratify the above mentioned critical properties in the fresh state and also meet the requirements of low shrinkage and high mechanical strength.

5.1 Flowability measurement

Concrete for 3D printing has to be as fluid as possible to be delivered easily in the pipe system. Meanwhile, it has to be stable to prevent the segregation during the flow.

(1) Slump-flow test

The slump-flow test has been used successfully over decades to measure the flowability of fresh concrete mixes with high flowability in unconfined conditions. This method is easy to handle in laboratories and on site mostly due to its simplicity, low cost, and immediate results. Slump-flow test performing is according to the procedure recommended by EFNARC committee (European Federation for Specialist Construction Chemicals and Concrete Systems) [104]. In this test, a slump cone as illustrated in Fig. 5 (a) is filled with concrete. Then the cone is removed. The average diameter of the spread concrete in two perpendicular directions is assesses to determine the workability. It is noteworthy that the slump-flow test is different from the slump test which is regulated by EN 12350-2 [105]. The former is suitable to characterize the concrete of high flowability by the spreading diameter of concrete when lifting the filled cone (Fig. 5(b)). While the latter is used to describe the concrete of relative low flowability by the drop in height of concrete after the cone is removed (Fig. 5(c)).

(2) T_{50} slump test

T_{50} slump test is also used to evaluate the fluidity of fresh concrete. T_{50} flow time is obtained from the test, which simply refers to duration time taken by the concrete to flow to a diameter of 50 cm. T_{50} slump test provides additional information about segregation resistance and uniformity of concrete which can be achieved from the visual observations during the test and/or measurement of T_{50} time. Acceptable T_{50} times range from 2 to 5 second. According to EFNARC [104], there are three typical slump flow classes for the range of applications, as listed in Table 3.

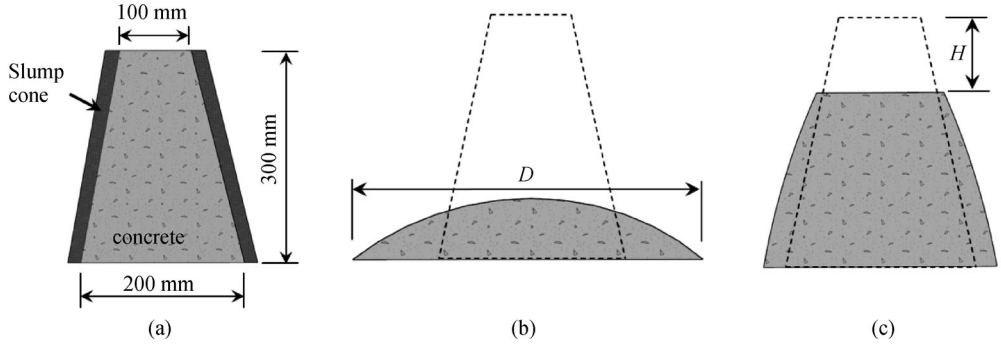

Fig. 5 (a) Slump cone filled with fresh concrete; (b) spreading diameter of concrete; (c) drop in height of concrete when lifting the filled cone

(3) V-funnel test

V-funnel test is used to evaluate the viscosity of fresh concrete and the deformability to pass through restricted areas by the V-funnel flow time. In this test, the V-shaped funnel shown in Fig. 6 is filled with fresh concrete. The elapsed time between opening the bottom outlet and complete emptying of the funnel is specified as the V-funnel flow time (V_t). The value of V_t is associated with viscosity, interparticle friction or blockage of flow [106]. The concrete for 3D printing shall perform well with no significant segregation and jamming when pass through the narrow opening.

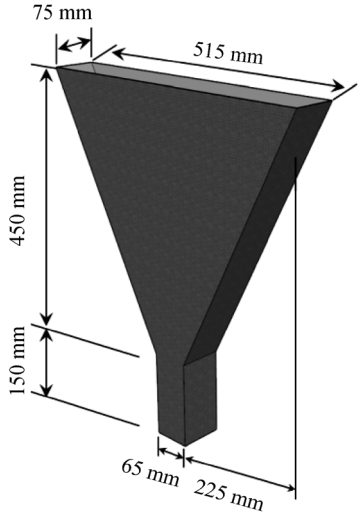

Fig. 6 Sketch of V-funnel used for flowability measurement

(4) L-box testing

The L-Box test is employed to evaluate the flowable performance and in particular the passing ability of concrete mixtures. Results obtained from this test can be used to assess the passing ability of concrete flow through narrow pipes in the printing system and small openings formed by the deposition head. Fig. 7 shows the apparatus sketching of L-box test. At first, the vertical section is filled with fresh concrete. When lifted up the slide gate between the two sections, concrete will flow into the horizontal section through the opening of obstructing bars. After the flow stopped, the height of concrete remaining in the vertical section is marked as H_1 and in the horizontal section is marked as H_2. The L-box value is simply defined as the height ratio of H_1/H_2, which is an indicator of concrete passing ability. Viscosity classifications of fresh concrete could be specified by bot V-funnel and T50 slump flow times as presented in Table 3.

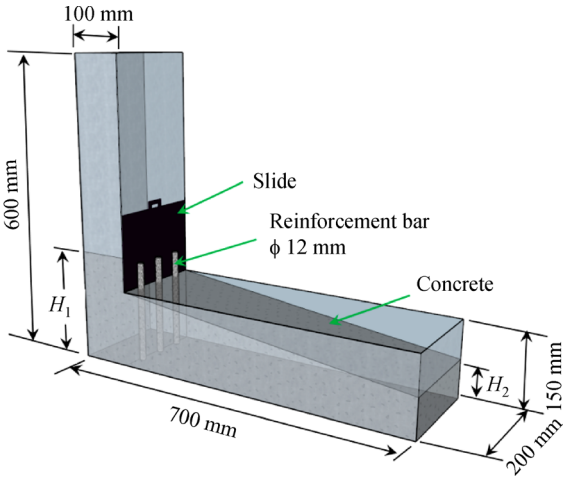

Fig. 7 Sketching of test apparatus of L-box

5.2 Rheology property measurement

Rheology property determines the workability and compaction ability of fresh concrete. The slump flow test cannot be applied to characterize concrete of low viscosity or high flowability. Viscosity behaviour of concrete mixture can be measured by digital viscometers. Brookfield DV-E model viscometer is one type of commonly used rotational viscometer. The recorded viscosity and torque are easily and accurately displayed and output by the digital viscometer. Fig. 8 shows a schematic view of rheometer used for rheology measurement. Viscosity measurement of concrete mortars was conducted at different rotational speeds. For example, the measurements were conducted at the seven rotational speeds, i.e., 1, 2.5, 5, 10, 20, 50, and 100 rpm at 0, 20 and 40 min after mixing [107]. The viscous behaviour can be characterized from the relationship between the torque and the rotational speed obtained from the rheometer [68]. It worth noting that the time dependent viscosity of the concretes is needed to be determined so as to provide complementary information to the rheology property prevent the inaccurate yield stress [37]. The viscous behaviour is apparent at a low rotational speed. However, the blade in viscometer at high rotation rates produces shear thinning effect which breaks down the formation of high viscous behaviour of mixture, causing a dominant flowable behaviour. When preparing the concrete for 3D printing, the flowable or viscous property of mixture can be adjusted by the rotational speed of used blender.

5.3 Setting and hardening measurement

Setting property monitoring is of great significance to control the printing process. Setting behaviour refers to the fluidity and stiffness change of concrete right from casting to final hardening. Setting times are important parameters

Table 3 Slump flow, viscosity, and passing ability classes according to EFNARC [104]

Slump flow classes	Slump flow diameter (mm)	Viscosity classes	T50 time (s)	V-funnel time (s)	Passing ability classes	L-box height ratio (H_1/H_2)
SF1	550–650	VF1	⩽2	⩽8	PA1	⩾0.8 with two rebar
SF2	660–750	VF2	>2	9–25	PA2	⩾0.8 with three rebar
SF3	760–850					

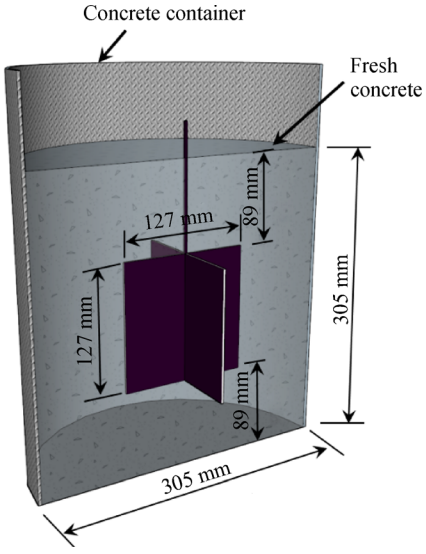

Fig. 8 Schematic view of rheometer used for rheology measurement

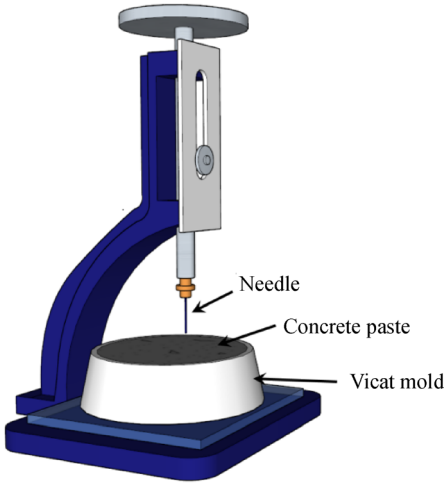

Fig. 9 Schematic illustration of Vicat device

related to strength gain and stiffness development of concretes.

(1) Vicat needle test

Vicat needle test is a standard method to characterize the setting and hardening of cement mortars. Initial and final setting times of fresh mixtures are determined according to the ASTM C 403/C 403M-99 [108]. As shown in Fig. 9, the mortar is placed in a 40 mm high Vicat mould. A needle with a 1 mm^2 cross section is fixed on a 300 g moveable rod and then falls down under gravity and penetrates the sample. Penetration depth versus elapsed time are recorded. This process is conducted repeatedly at regular time intervals until the final hardening of cement paste. The initial and final setting times are specified as the times at which the penetration depth reaches values of (39±0.5) mm and less than 0.5 mm, respectively. Fig. 10 depicts a typical penetration depth versus time recorded by a Vicatronic automatic apparatus. Sleiman et al. [109] developed a modified Vicat device, which allows to detect the setting behaviour evolution starting immediately after being casted. It is unlike the usually used Vicat measurement apparatus that cannot capture the change until initial set.

(2) Wave transmission method

Ultrasonic method offers an effective way for continually monitoring the setting performance of concrete. In 2000, Reinhardt firstly introduced an almost fully automated and easy-handled testing device which utilizes ultrasonic wave to continuously detect the setting process of concrete [111,112]. The method has been shown to be sensitive and reliable to monitor the hydration process of cement paste as affected by different w/c ratios, different curing temperatures, and different cement types and fineness [113].

A schematic of the wave transmission measurement is shown in Fig. 11. In this method, a container is filled with mortar or concrete. Primary or compression waves (P-waves) are generated by a transmitter and sent through the material and recorded by a receiver. The velocity V_p (km/s) can be used as an indicator for describing the setting and hardening progress of the test materials, which is calculated by Eqs. (1) and (2). Where $T_{concrete}$ and T_{water} account for the times of P-waves travel through the entire width of concrete and pure water (calibration), respectively; V_{water} indicates transmission velocity of ultrasonic waves in pure water, i.e., 1480 m/s; L (mm) is the width of the specimen and Δt (μs) is the travel time of ultrasonic pulse.

$$\Delta t = T_{concrete} - \left(T_{water} - \frac{L}{V_{water}}\right), \quad (1)$$

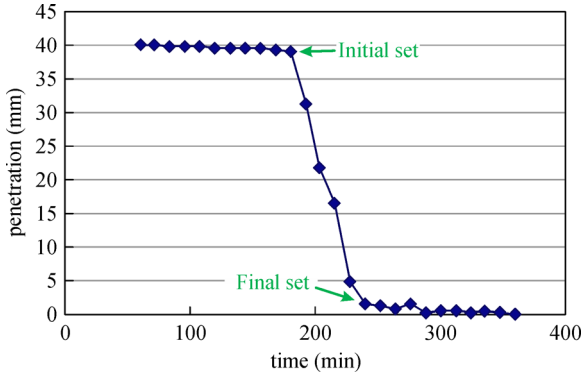

Fig. 10 Penetration depth versus time recorded by Vicatronic automatic apparatus [110]

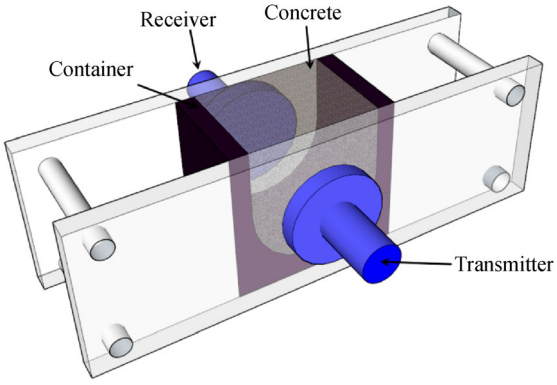

Fig. 11 Principle of P-wave transmission method

$$V_p = \frac{L}{\Delta t}. \tag{2}$$

The velocity of ultrasonic wave increases as concrete solidifies. It has been proved that the time required to traverse through the entire sample is directly related to the hydration degree [114]. The initial and final setting times of mortar can be ascertained from the relationship between pulse velocity (V_p) and the time after casting. As shown in Fig. 12, the setting process of concrete from liquid state to final hardening can be divided into three stages based on the V_p vs time curves. Moreover, the attenuation coefficient (α_p) of ultrasonic waves could also be used to characterize the hydration process of cement mortar. α_p is calculate with energy generated by the emitter (A), the energy detected by the receiver (R) and the energy transmission coefficient of the interface (T) [115]:

$$\alpha_p = -\frac{1}{L}\ln\left(\frac{R}{AT_1T_2}\right). \tag{3}$$

(3) Wave reflection method

Recently, ultrasonic wave reflection method has been proved to be effective to monitor the early age setting and

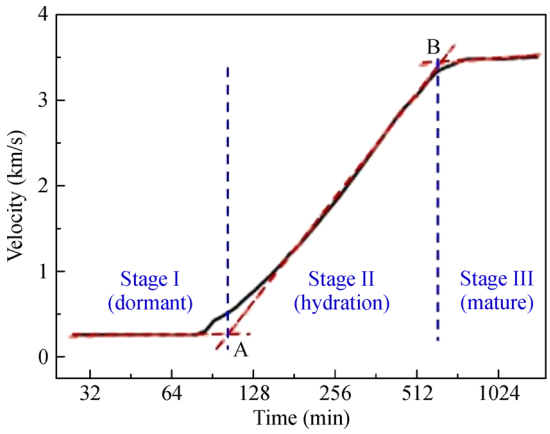

Fig. 12 Typical curve of wave velocity evolution at early age

hardening process of concretes non-destructively and continuously [116]. Different with wave transmission method, the reflection technique utilizes a single transducer that acts both as transmitter and receiver. The transducer records the reflection loss of transverse or shear waves (S-waves) at an interface between a steel plate and the concrete. Fig. 13 illustrates a schematic view of the experimental set-up. S-waves can only propagate in solids. When the mortar is under fresh state, the entire S-wave pulse would be reflected back from the interface between two distinct different materials. As the gradually hardening of concrete, its ability to transmit wave pulse increases, resulting in the wave pulse is partly reflected from the interface. Therefore, it is feasible to relate the hydration degree of testing mortar with the amplitude of lost waves. When the mortar comes into a mature stage, the reflection coefficient turns to a constant value [117]. The investigations conducted so far have demonstrated that the wave reflection method is reliable and accurate to identify the differences in the setting behaviour of concretes caused by factors such as retarding or accelerating agent as well as curing temperatures.

Additionally, specific points in the wave velocity gradient curves obtained from ultrasonic measurement can also be employed for setting time determination. As shown in Fig. 14, the point δV_p^{max} corresponds to the time when penetration resistance (P_r) starts to increase. The point δV_s^{max} is observed around the initial setting time (t_i). This increase of E_d gradient between the point δV_s^{max} and δE_d^{max} curve reflects the rapid volume increase in C–S–H to cement hydration. And δE_d^{max} is related to the time of final setting occur. Based on these specific points, the setting behaviour can be decomposed into four stages: dormant period, initial percolation, setting and early stage hardening [117].

5.4 Strength measurement

The evaluation of early age mechanical properties of concrete is a challenging task. Early-age strength devel-

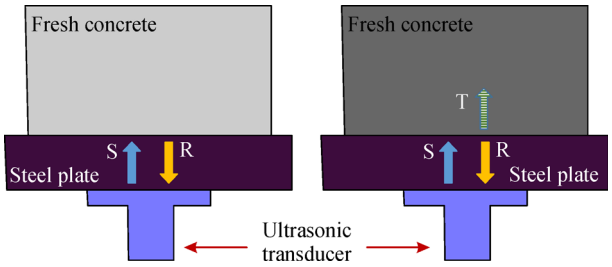

Fig. 13 Principle of S-wave reflection method

opment of concrete for 3D printing is critical to the buildability control and engineering application of utilized materials. Strength or stiffness development is related to transition process of mortars from plastic and deformable to hardened state.

(1) Ultrasonic method

One alternative approach to monitor the early-age strength of concrete is using wave propagation techniques as presented in Section 5.3. The transmit velocity and reflection loss of ultrasonic pulse is sensitive to the hydration degree of concrete, both of which are direct related to the strength of concrete. It is therefore feasible to use the ultrasonic pulse information to evaluate and predict the strength gain of cement mortar. Dynamic elastic parameters, the dynamic Poisson's ratio ν_d and the dynamic Young's modulus E_d are calculated with the parameters of P-wave velocity V_P, S-wave V_S velocity and the density of concrete ρ as the following equations [118]:

$$\nu_d = 1-2(V_s^2/V_p^2), \tag{4}$$

$$E_d = V_p^2\rho\frac{(1+\nu_d)(1-2\nu_d)}{(1-\nu_d)}. \tag{5}$$

Fig. 15 shows a direct comparison of normalized S-wave reflection and strength development of three types of concrete. It is reliable to assess the compressive strength by means of ultrasonic technique. Boumiz et al. [119] developed an integrated approach of ultrasonic, calorimetric, and conduct metric techniques, which were applied simultaneously to the same batches of cement pastes and mortars. Young's modulus of elasticity and Poisson's ratio were studied as functions of time and of degree of hydration. Akkaya [120] stated that the compressive strength development at early ages was linearly related to the energy loss of reflection waves at the interface between plate and concrete specimen. This linear correlation would not be affected by different curing temperature, mix design and material type. Once the relationship between reflection loss and concrete strength is calibrated, it can be used to predict the concrete strength at early ages based on the ultrasonic data. Voigt et al. [117,121] has established a relation between the ability of concrete materials to transmit ultrasonic waves and their early-age compressive strength. Demirboga et al. [122] demonstrated an exponential relationship between ultrasonic pulse velocity and compressive strength of concrete mixed with fly ash and blast furnace slag.

(2) Transducer technique

The hydration process of cement composite is a complex, exothermic chemical reaction. The degree of hydration reaction is greatly related to the amount of reaction heat produced in the hydration process. Therefore, it is feasible to evaluate the hydration process by monitoring the thermal information through fibre optical sensors or thermocouples. Wang et al. [124] have used a new type of piezoelectric lead zirconate titanate (PZT) impedance transducer to monitor the compressive strength gain. The transducer was embedded in the fresh casted concrete and the mechanical strength was predicted based on the PZT

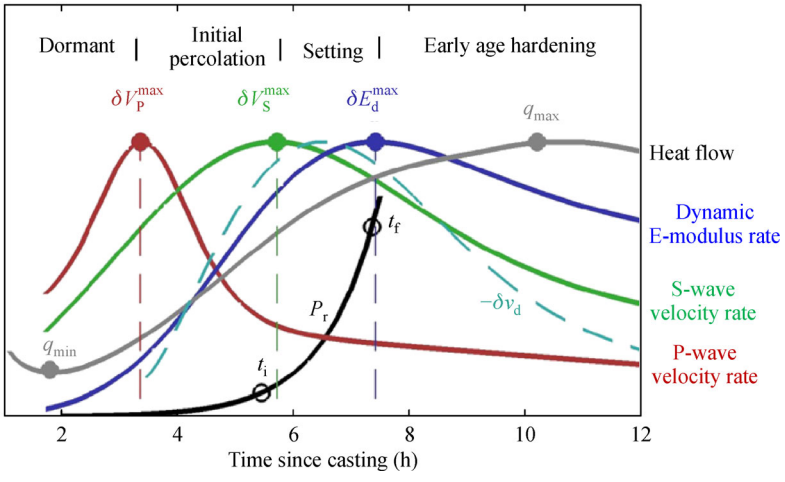

Fig. 14 Gradient curves of heat flow, penetration resistance (black curve) and V_P, V_S and E_d on mortar [117]

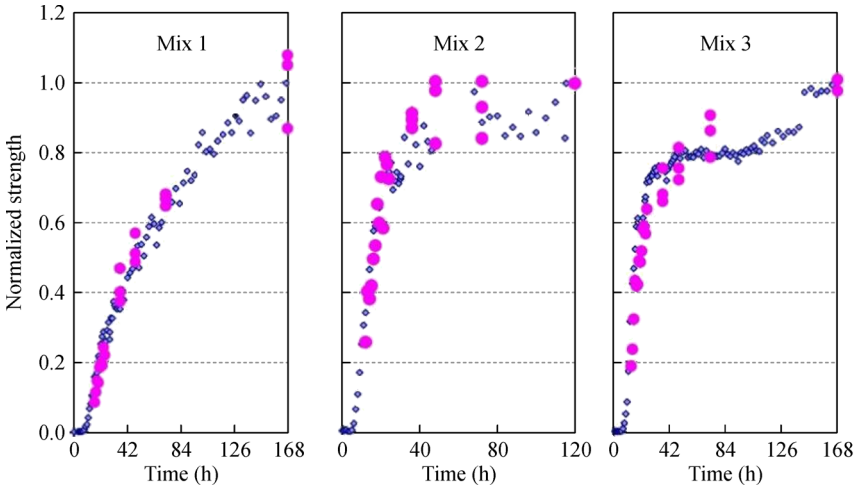

Fig. 15 Comparison of normalized S-wave reflection (blue points) and strength gain (magenta points) of concrete compositions with strength of 26, 37 and 55 MPa, respectively [123]

admittance (inversion of impedance) signals. Gu et al. [125] carried out early-age strength monitoring of concrete through placing piezoelectric transducers which were in the form of "smart aggregates". Cai et al. [126] carried out a fibre optical sensing technology to record the change of temperature and crack of a dam. Lin et al. [127] have applied fibre Bragg grating (FBG) sensors to detect the hydration temperature during the hardening process of a pre-stressed concrete (PC) beam.

5.5 Shrinkage measurement

(1) Free shrinkage test

Drying shrinkage is determined in accordance with the standard of ASTM C157-75 [128]. Specimens used for monitor the free shrinkage are prisms, the length of which is far bigger than its width and height. Fig. 16 shows the measuring method of autogenous shrinkage. The dimension of prism can be 70 mm × 70 mm × 280 mm or 50 mm × 50 mm × 300 mm. Before casting, Teflon sheets were placed inside the steel mould to eliminate the constraint of concrete from the mould. An alternative practice is applying lubricating oil. A dial gage extensometer was horizontally embedded in the middle of specimen. Polyester film or plastic wrap was utilized to prevent moisture evaporation from the top surface. The gage is utilized to record the length change of prism specimen. The relationship of one-dimensional drying shrinkage strain versus time can be obtained. Specimens were cured for 24 h at 20 °C and 100% relative humidity and then are demoulded [129].

The standard method employing gage extensometers belongs to a type of averaged shrinkage measurements. Moreover, internal shrinkage at specific points can be monitored by embedding sensors in the concrete, such as strain gauges and fibre optics [130]. Yılmazturka et al. [131] proposed a digital photogrammetric method to detect the shrinkage in concrete specimens. This optical method belongs to a full-field measurement. Similarly, Chen et al. [132] have developed an automated Moiré fringe analysis system by means of Cure Reference Method. Shrinkage evolution could be determined as a function of location, time, humidity and temperature. Newlands et al. [133] developed a new linear test method which utilized a triangular mould to measure the unrestrained shrinkage in concrete at early ages.

(2) Restrained shrinkage test

A ring-type specimen is used to detect the restrained shrinkage of concrete according to ASTM C 1581 [134]. After casting, specimens are cured at 20 °C for 24 h and 100% relative humidity. After that, the outer steel ring would be stripped off. In order to make the drying only take place on the outer circumferential surface, the top surface of the concrete ring was instantly covered by silicon rubber or vinyl to prevent drying. After that, the specimens are exposed to drying in a humidity cabinet at (23±2) °C and (50±5) % relative humidity. Fig. 17 shows the schematic description of restrained shrinkage test method and dimensions of the ring mould. The shrinkage was determined by the crack width. Gesoglu et al. [135] proposed a special microscope setup to measure the crack width on constrained ring specimens.

6 Design and evaluation method

Nazari [136] investigated the effect of six factors on the compressive strength of geopolymers at four levels according to the L32 array proposed by genetic program-

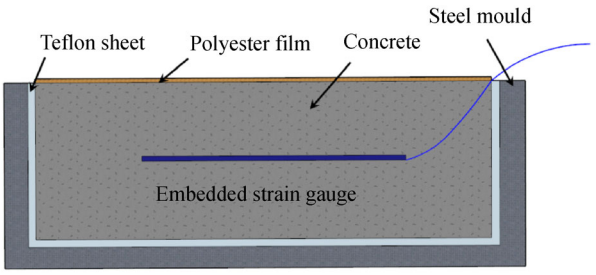

Fig. 16 Schematic description of the autogenous shrinkage testing

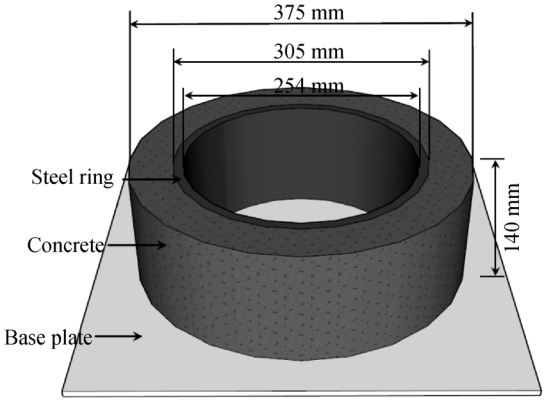

Fig. 17 Sketch of restrained shrinkage ring specimen

ming. Sonebi [137] carried out a factorial design to mathematically identify the relative significance of four mix parameters including the cement and fly ash content, water to powder ration and dosage of superplasticizer and their coupled effects on the fresh performance and compressive strength of self-compacting concrete. Feng et al. [15] proposed a parabolic failure criterion for orthotropic 3D printed structure of cementitious materials based on the maximum stress criterion by taking into the tested parameters of maximum stress, initial elastic modulus, strain under peak load and the ultimate strain. Ahmer et al. [138] have adopted Taguchi method to analyse the effects of four parameters on the setting time of fly ash based geopolymers. Shadi et al. [139] have evaluated the influence of three factors, including 3 levels of curing temperature, 3 levels of oven curing time and 3 levels of NaOH concentration, on the mechanical strength of geopolymers by utilizing Taguchi method.

7 Conclusion

3D printing of concrete material is a promising method that may revolutionize the traditional building and construction processes in terms of apparent benefits in low-cost, high-efficient automatic construction, architectural design freedom, and reduction of labour requirement and risks during construction. This paper has summarized the raw materials usually adopted in concrete manufaction and their physical characteristics. The concrete mixture for 3D printing shall possess favourable printable properties, which can be controlled and optimized through adjusting the type and content of powder mixtures and chemical additives. Preparation of concrete material compatible with large-scale 3D printing is a complex work. There are various inter-related influencing factors that govern the final fresh and hardening performances of concrete mixture. Detail investigation and comprehensive consideration of the impacting mechanism of each constitute and chemical additive on the workability are significantly recommended for the preparation design of printable concrete. Meanwhile, employing various experimental devices to measure and evaluate the fresh and hardened properties of concrete material will facilitate the model design, realize a smooth printing process and ensure good stiffness and durability of concrete for 3D printing. Although still in the proof of concept and preliminary manufacturing stages, it is promising that 3D concrete printing can reach its maximum potential in the construction field.

Acknowledgements The authors are grateful to the support by the National Major Research Instrument Development Project of the National Natural Science Foundation of China (Grant No. 51627812), and the opening project of State Key Laboratory of Explosion Science and Technology (Beijing Institute of Technology, Grant No. KFJJ13-11M).

References

1. Singh M, Haverinen H M, Dhagat P, Jabbour G E. Inkjet printing-process and its applications. Advanced Materials, 2010, 22(6): 673–685
2. Labonnote N, Ronnquist A, Manum B, Rüther P. Additive construction: State-of-the-art, challenges and opportunities. Automation in Construction, 2016, 72: 347–366
3. Khoshnevis B, Dutton R. Innovative rapid prototyping process makes large sized, smooth surfaced complex shapes in a wide variety of materials. Materials Technology, 1998, 13(2): 53–63
4. Dini E. Design of D-shape printers, Monolite UK Ltd, 2007
5. Kira. WinSun China builds world's first 3D printed villa and tallest 3D printed apartment building. 3D printer and 3D printing news, 2015
6. Rudenko A. 3D printed concrete castle is complete. 3D Concrete House Printer, 2015
7. Massimo M. The clay and straw wall by the 3 meters. World Advanced Saving Project, 2016
8. Gibbons G J, Williams R, Purnell P, Farahi E. 3D Printing of cement composites. Advances in Applied Ceramics, 2010, 109(5): 287–290
9. Maier A K, Dezmirean L, Will J, Greil P. Three-dimensional printing of flash-setting calcium aluminate cement. Journal of Materials Science, 2011, 46(9): 2947–2954

10. Xia M, Sanjayan J. Method of formulating geopolymer for 3D printing for construction applications. Materials & Design, 2016, 110: 382–390
11. Khoshnevis B, Bukkapatnam S, Kwon H, Saito J. Experimental investigation of contour crafting using ceramics materials. Rapid Prototyping Journal, 2001, 7(1): 32–42
12. Perrot A, Rangeard D, Pierre A. Structural built-up of cement-based materials used for 3D-printing extrusion techniques. Materials and Structures, 2016, 49(4): 1213–1220
13. Nerella V N, Krause M, Nather M. Studying printability of fresh concrete for formwork free concrete on-site 3D printing technology (CONPrint3D). In: Proceeding for 25th conference on rheology of building materials, Regensburg, Germany, 2016
14. Lim S, Buswell R A, Le T T, Austin S A, Gibb A G F, Thorpe T. Developments in construction-scale additive manufacturing processes. Automation in Construction, 2012, 21: 262–268
15. Feng P, Meng X, Chen J F, Ye L. Mechanical properties of structures 3D printed with cementitious powders. Construction & Building Materials, 2015, 93: 486–497
16. Gosselin C, Duballet R, Roux P, Gaudillière N, Dirrenberger J, Morel P. Large-scale 3D printing of ultra-high performance concrete–a new processing route for architects and builders. Materials & Design, 2016, 100: 102–109
17. Mazloom M, Ramezanianpour A A, Brooks J J. Effect of silica fume on mechanical properties of high-strength concrete. Cement and Concrete Composites, 2004, 26(4): 347–357
18. Aqel M, Panesar D K. Hydration kinetics and compressive strength of steam-cured cement pastes and mortars containing limestone filler. Construction & Building Materials, 2016, 113: 359–368
19. Brooks J J, Megat Johari M A, Mazloom M. Effect of admixtures on the setting times of high-strength concrete. Cement and Concrete Composites, 2000, 22(4): 293–301
20. Bouzoubaâ N, Lachemi M. Self-compacting concrete incorporating high volumes of class F fly ash. Cement and Concrete Research, 2001, 31(3): 413–420
21. Plank J, Winter C. Competitive adsorption between superplasticizer and retarder molecules on mineral binder surface. Cement and Concrete Research, 2008, 38(5): 599–605
22. Agarwal S K, Masood I, Malhotra S K. Compatibility of superplasticizers with different cements. Construction & Building Materials, 2000, 14(5): 253–259
23. Nkinamubanzi P C, Aitcin P C. Cement and superplasticizer combinations: compatibility and robustness. Cement, Concrete and Aggregates, 2004, 26(2): 1–8
24. Lachemi M, Hossain K M A, Lambros V, Nkinamubanzi P C, Bouzoubaâ N. Performance of new viscosity modifying admixtures in enhancing the rheological properties of cement paste. Cement and Concrete Research, 2004, 34(2): 185–193
25. Soroka I. The determination of setting time of portland cement by the vicat test. Cement and Concrete Research, 1984, 14(6): 884–886
26. Valič M I. Hydration of cementitious materials by pulse echo USWR: Method, apparatus and application examples. Cement and Concrete Research, 2000, 30(10): 1633–1640
27. Kamada T, Uchida S, Rokugo K. Nondestructive evaluation of setting and hardening of cement paste based on ultrasonic propagation characteristics. Journal of Advanced Concrete Technology, 2005, 3(3): 343–353
28. Voigt T, Grosse C U, Sun Z, Shah S P, Reinhardt H W. Comparison of ultrasonic wave transmission and reflection measurements with P- and S-waves on early age mortar and concrete. Materials and Structures, 2005, 38(282): 729–738
29. Sharma S, Mukherjee A. Monitoring freshly poured concrete using ultrasonic waves guided through reinforcing bars. Cement and Concrete Composites, 2015, 55: 337–347
30. Sharma S, Mukherjee A. Ultrasonic guided waves for monitoring the setting process of concretes with varying workabilities. Construction & Building Materials, 2014, 72: 358–366
31. Liu S, Zhu J, Seraj S, Cano R, Juenger M. Monitoring setting and hardening process of mortar and concrete using ultrasonic shear waves. Construction & Building Materials, 2014, 72: 248–255
32. Rengier F, Mehndiratta A, von Tengg-Kobligk H, Zechmann C M, Unterhinninghofen R, Kauczor H U, Giesel F L. 3D printing based on imaging data: review of medical applications. International Journal of Computer Assisted Radiology and Surgery, 2010, 5(4): 335–341
33. Kaye R, Goldstein T, Zeltsman D, Grande D A, Smith L P. Three dimensional printing: A review on the utility within medicine and otolaryngology. International Journal of Pediatric Otorhinolaryngology, 2016, 89: 145–148
34. Khoshnevis B, Hwang D, Yao K T. Mega-scale fabrication by contour crafting. International Journal of Industrial and Systems Engineering, 2006, 1: 301–320
35. Güneyisi E, Gesoglu M, Ozturan T. Properties of rubberized concretes containing silica fume. Cement and Concrete Research, 2004, 34(12): 2309–2317
36. Lange F, Mortel H, Rudert V. Dense packing of cement pastes and resulting consequences on mortar properties. Cement and Concrete Research, 1997, 27(10): 1481–1488
37. Felekoğlu B, Tosun K, Baradan B, Altun A, Uyulgan B. The effect of fly ash and limestone fillers on the viscosity and compressive strength of self-compacting repair mortars. Cement and Concrete Research, 2006, 36(9): 1719–1726
38. Sanchez F, Sobolev K. Nanotechnology in concrete – A review. Construction & Building Materials, 2010, 24(11): 2060–2071
39. Siddique R. Utilization of silica fume in concrete: Review of hardened properties. Resources, Conservation and Recycling, 2011, 55(11): 923–932
40. Zhang Z, Zhang B, Yan P. Comparative study of effect of raw and densified silica fume in the paste, mortar and concrete. Construction & Building Materials, 2016, 105: 82–93
41. Zhang M, Tam C, Leow M. Effect of water-to-cementitious materials ratio and silica fume on the autogenous shrinkage of concrete. Cement and Concrete Research, 2003, 33(10): 1687–1694
42. Jones M R, McCarthy A, Booth A P P G. Characteristics of the ultrafine component of fly ash. Fuel, 2006, 85(16): 2250–2259
43. Güneyisi E. Fresh properties of self-compacting rubberized concrete incorporated with fly ash. Materials and Structures, 2010, 43(8): 1037–1048
44. Pal S, Mukherjee A, Pathak S. Investigation of hydraulic activity of ground granulated blast furnace slag in concrete. Cement and

Concrete Research, 2003, 33(9): 1481–1486
45. Gürol G. Components for Economic Concrete, cement/water/fine and coarse aggregate/chemical and mineral admixtures. Journal of Design and Construction, 1999, 164: 66–74
46. Turker P, Yesilkaya A, Yeginobalı A. The hydration process and microstructural development of limestone Portland cements. Cem Concr World, 2004, 48: 50–66
47. Sobolev K, Gutierrez M F. How nanotechnology can change the concrete world. American Ceramic Society Bulletin, 2005, 84: 14–17
48. Björnström J, Martinelli A, Matic A, Börjesson L, Panas I. Accelerating effects of colloidal nano-silica for beneficial calcium–silicate–hydrate formation in cement. Chemical Physics Letters, 2004, 392(1-3): 242–248
49. Li H, Xiao H G, Yuan J, Ou J. Microstructure of cement mortar with nano-particles. Composites. Part B, Engineering, 2004, 35(2): 185–189
50. Wongkornchaowalit N, Lertchirakarn V. Setting time and flowability of accelerated Portland cement mixed with polycarboxylate superplasticizer. Journal of Endodontics, 2011, 37(3): 387–389
51. Zhang D F, Ju B Z, Zhang S F, He L, Yang J Z. The study on the dispersing mechanism of starch sulfonate as a water-reducing agent for cement. Carbohydrate Polymers, 2007, 70(4): 363–368
52. El-Gamal S M A, Al Nowaiser F M, Al Baity A O. Effect of superplasticizers on the hydration kinetic and mechanical properties of Portland cement pastes. Journal of Advanced Research, 2012, 3(2): 119–124
53. Chandra S, Bjornström J. Influence of cement and superplasticizers type and dosage on the fluidity of cement mortars—Part I. Cement and Concrete Research, 2002, 32(10): 1605–1611
54. Zingg A, Winnefeld F, Holzer L, Pakusch J, Becker S, Figi R, Gauckler L. Interaction of polycarboxylate-based superplasticizers with cements containing different C3A amounts. Cement and Concrete Composites, 2009, 31(3): 153–162
55. Gołaszewski J, Szwabowski J. Influence of superplasticizers on rheological behaviour of fresh cement mortars. Cement and Concrete Research, 2004, 34(2): 235–248
56. Zhang M H, Sisomphon K, Ng T S, Sun D J. Effect of superplasticizers on workability retention and initial setting time of cement pastes. Construction & Building Materials, 2010, 24(9): 1700–1707
57. Chandra S, Bjornstrom J. Influence of superplasticizer type and dosage on the slump loss of Portland cement mortars—Part II. Cement and Concrete Research, 2002, 32(10): 1613–1619
58. Salvador R P, Cavalaro S H P, Segura I, Figueiredo A D, Pérez J. Early age hydration of cement pastes with alkaline and alkali-free accelerators for sprayed concrete. Construction & Building Materials, 2016, 111: 386–398
59. Lin X Q, Zhang T, Huo L. Preparation and application of cement-based 3D printing materials in construction. In: The 9th session of the general assembly and the 11th national symposium on concrete and cement products branch of China silicate society, 2015: 175–180 (in Chinese)
60. Zhang G, Li G, Li Y. Effects of superplasticizers and retarders on the fluidity and strength of sulphoaluminate cement. Construction & Building Materials, 2016, 126: 44–54
61. Claisse P A. L P, Omari M. A. Workability of cement pastes. ACI Materials Journal, 2001, 98: 476–482
62. Lee S H, Kim H J, Sakai E, Daimon M. Effect of particle size distribution of fly ash–cement system on the fluidity of cement pastes. Cement and Concrete Research, 2003, 33(5): 763–768
63. Park C K, Noh M H, Park T H. Rheological properties of cementitious materials containing mineral admixtures. Cement and Concrete Research, 2005, 35(5): 842–849
64. Burgos-Montes O, Palacios M, Rivilla P, Puertas F. Compatibility between superplasticizer admixtures and cements with mineral additions. Construction & Building Materials, 2012, 31: 300–309
65. Grzeszczyk S, Lipowski G. Effect of content and particle size distribution of high-calcium fly ash on the rheological properties of cement pastes. Cement and Concrete Research, 1997, 27(6): 907–916
66. Kwan A, Wong H. Effects of packing density, excess water and solid surface area on flowability of cement paste. Advances in Cement Research, 2008, 20(1): 1–11
67. Mastali M, Dalvand A. Use of silica fume and recycled steel fibers in self-compacting concrete (SCC). Construction & Building Materials, 2016, 125: 196–209
68. Güneyisi E, Gesoglu M, Al Goody A, İpek S. Fresh and rheological behavior of nano-silica and fly ash blended self-compacting concrete. Construction & Building Materials, 2015, 95: 29–44
69. Kong H J, Bike S G, Li V C. Development of a self-consolidating engineered cementitious composite employing electrosteric dispersion/stabilization. Cement and Concrete Composites, 2003, 25 (3): 301–309
70. Mardani-Aghabaglou A, Tuyan M, Yılmaz G, Arıöz Ö, Ramyar K. Effect of different types of superplasticizer on fresh, rheological and strength properties of self-consolidating concrete. Construction & Building Materials, 2013, 47: 1020–1025
71. Singh S B, Munjal P, Thammishetti N. Role of water/cement ratio on strength development of cement mortar. J Build Eng, 2015, 4: 94–100
72. Leemann A, Winnefeld F. The effect of viscosity modifying agents on mortar and concrete. Cement and Concrete Composites, 2007, 29(5): 341–349
73. Li G, He T, Hu D, Shi C. Effects of two retarders on the fluidity of pastes plasticized with aminosulfonic acid-based superplasticizers. Construction & Building Materials, 2012, 26: 72–78
74. Silva Y F, Robayo R A, Mattey P E, Delvasto S. Properties of self-compacting concrete on fresh and hardened with residue of masonry and recycled concrete. Construction & Building Materials, 2016, 124: 639–644
75. Malaeb Z, Hachem H, Tourbah A, Maalouf T, Zarwi N E. 3D concrete printing: machine and mix design. International Journal of Civil Engineering, 2015, 6: 14–22
76. Le T T, Austin S A, Lim S, Buswell R A, Gibb A G F, Thorpe T. Mix design and fresh properties for high-performance printing concrete. Materials and Structures, 2012, 45(8): 1221–1232
77. Tang C, Yen T, Chen K. The rheological behavior of medium strength high performance concrete. Structural Engineering Mechamics & Computation, 2001, 2: 1373–1380

78. Benaicha M, Roguiez X, Jalbaud O, Burtschell Y, Alaoui A H. Influence of silica fume and viscosity modifying agent on the mechanical and rheological behavior of self compacting concrete. Construction & Building Materials, 2015, 84: 103–110
79. Robeyst N, Gruyaert E, Grosse C U, De Belie N. Monitoring the setting of concrete containing blast-furnace slag by measuring the ultrasonic p-wave velocity. Cement and Concrete Research, 2008, 38(10): 1169–1176
80. Gesoglu M, Ozbay E. Effects of mineral admixtures on fresh and hardened properties of self-compacting concretes: binary, ternary and quaternary systems. Materials and Structures, 2007, 40(9): 923–937
81. Paglia C, Wombacher F, Bohni H. The influence of alkali-free and alkaline shotcrete accelerators within cement systems. Cement and Concrete Research, 2001, 31(6): 913–918
82. Maltese C, Pistolesi C, Bravo A, Cella F, Cerulli T, Salvioni D. A case history: Effect of moisture on the setting behaviour of a Portland cement reacting with an alkali-free accelerator. Cement and Concrete Research, 2007, 37(6): 856–865
83. Galobardes I, Salvador R P, Cavalaro S H P, Figueiredo A, Goodier C I. Adaptation of the standard EN 196-1 for mortar with accelerator. Construction & Building Materials, 2016, 127: 125–136
84. Gesoglu M, Guneyisi E. Strength development and chloride penetration in rubberized concretes with and without silica fume. Materials and Structures, 2007, 40(9): 953–964
85. Zelic J, Rusic D, Vea D, Krstuloric R. The role of silica fume in the kinetics and mechanisms during the early stage of cement hydration. Cement and Concrete Research, 2000, 30(10): 1655–1662
86. Li G. Properties of high-volume fly ash concrete incorporating nano-SiO_2. Cement and Concrete Research, 2004, 34(6): 1043–1049
87. Ye Q, Zhang Z, Kong D, Chen R. Influence of nano-SiO_2 addition on properties of hardened cement paste as compared with silica fume. Construction & Building Materials, 2007, 21(3): 539–545
88. Ye Q, Zhang Z, Sheng L, Chen R. A comparative study on the pozzolanic activity between nano-SiO2 and silica fume. J Wuhan Univ Tech-Mater Sci Ed, 2006, 21(3): 153–157
89. Jo B W, Kim C H, Tae G H, Park J B. Characteristics of cement mortar with nano-SiO_2 particles. Construction & Building Materials, 2007, 21(6): 1351–1355
90. Malhotra V M, Zhang M H, Read P H. Long-term mechanical properties and durability characteristics of high-strength/high-performance concrete incorporating supplementary cementing materials under outdoor exposure conditions. ACI Materials Journal, 2000, 97: 518–525
91. Liu B, Xie Y, Zhou S, Yuan Q. Influence of ultrafine fly ash composite on the fluidity and compressive strength of concrete. Cement and Concrete Research, 2000, 30(9): 1489–1493
92. Ghezal A, Khayat K H. Optimizing self-consolidating concrete with limestone filler by using statistical factorial design methods. Materials Journal, 2002, 99: 264–272
93. Lee S J, Won J P. Shrinkage characteristics of structural nano-synthetic fibre-reinforced cementitious composites. Comp Struct, 2016, 157: 236–243
94. Bissonnette B, Attiogbe E K, Miltenberger M A, Fortin C. Drying shrinkage, curling, and joint opening of slabs-on-ground. ACI Materials Journal, 2007, 104: 259–267
95. Zhang J, Gong C, Guo Z, Zhang M. Engineered cementitious composite with characteristic of low drying shrinkage. Cement and Concrete Research, 2009, 39(4): 303–312
96. Khatib J M. Performance of self-compacting concrete containing fly ash. Construction & Building Materials, 2008, 22(9): 1963–1971
97. Rongbing B, Jian S. Synthesis and evaluation of shrinkage-reducing admixture for cementitious materials. Cement and Concrete Research, 2005, 35(3): 445–448
98. Guneyisi E, Gesoglu M, Karaoglu S, Mermerdaş K. Strength, permeability and shrinkage cracking of silica fume and metakaolin concretes. Construction & Building Materials, 2012, 34: 120–130
99. Al-Khaja W A. Strength and time-dependent deformations of silica fume concrete for use in Bahrain. Construction & Building Materials, 1994, 8(3): 169–172
100. Li J, Yao Y. A study on creep and drying shrinkage of high performance concrete. Cement and Concrete Research, 2001, 31 (8): 1203–1206
101. Mazloom M, Ramezanianpour A, Brooks J. Effect of silica fume on mechanical properties of high-strength concrete. Cement and Concrete Composites, 2004, 26(4): 347–357
102. Sellevold E J. The function of condensed silica fume in high strength concrete. In: Proceedings of international conference on utilization of high strength concrete, 1987, 4: 11–14
103. Shh S, Krguller M, Sarigaphuti M. Effects of shrinkage-reducing admixtures on restrained shrinkage cracking of concrete. ACI Materials Journal, 1992, 89: 289–295
104. EFNARC. The European Guidelines for Self-Compacting Concrete. Self-Compacting Concrete Guidelines, 2005
105. EN B. 12350-2 Testing fresh concrete. Slump-test. British Standard Institute, London, 2009
106. Lachemi M, Hossain K M A, Lambros V, Nkinamubanzi P C, Bouzoubaâ N. Self-consolidating concrete incorporating new viscosity modifying admixtures. Cement and Concrete Research, 2004, 34(6): 917–926
107. Shi Y X, Matsui I, Guo Y J. A study on the effect of fine mineral powders with distinct vitreous contents on the fluidity and rheological properties of concrete. Cement and Concrete Research, 2004, 34(8): 1381–1387
108. ASTM C. 403/403M-99. Standard test methods for time of setting of concrete mixtures by penetration resistance. Annual book of ASTM standards, 1999, 4: 1–6
109. Sleiman H, Perrot A, Amziane S. A new look at the measurement of cementitious paste setting by Vicat test. Cement and Concrete Research, 2010, 40(5): 681–686
110. Ylmen R, Jaglid U, Steenari B M, Panas I. Early hydration and setting of Portland cement monitored by IR, SEM and Vicat techniques. Cement and Concrete Research, 2009, 39(5): 433–439
111. Reinhardt H W, Grobe C U, Herb A T. Ultrasonic monitoring of setting and hardening of cement mortar—A new device. Materials and Structures, 2000, 33(9): 581–583
112. Reinhardt H W, Grosse C U. Continuous monitoring of setting and hardening of mortar and concrete. Construction & Building

Materials, 2004, 18(3): 145–154
113. Trtnik G, Turk G, Kavcic F, Bosiljkov V B. Possibilities of using the ultrasonic wave transmission method to estimate initial setting time of cement paste. Cement and Concrete Research, 2008, 38 (11): 1336–1342
114. Boumiz A, Vernet C, Tenoudji F C. Mechanical properties of cement pastes and mortars at early ages. Advanced Cement Based Materials, 1996, 3: 94–106
115. Li Z. Advanced concrete technology. John Wiley & Sons, 2011.
116. Oztfirk T, Rapoport J R, Popovics J S, Shah S P. Monitoring the setting and hardening of cement-based materials with ultrasound. Concrete Science and Engineering, 1999, 1(2): 83–91
117. Voigt T, Malonn T, Shah S P. Green and early age compressive strength of extruded cement mortar monitored with compression tests and ultrasonic techniques. Cement and Concrete Research, 2006, 36(5): 858–867
118. Carette J, Staquet S. Monitoring the setting process of eco-binders by ultrasonic P-wave and S-wave transmission velocity measurement: Mortar vs concrete. Construction & Building Materials, 2016, 110: 32–41
119. Boumiz A, Vernet C, Tenoudji F C. Mechanical properties of cement pastes and mortars at early ages: Evolution with time and degree of hydration. Advanced Cement Based Materials, 1996, 3: 94–106
120. Akkaya Y, Voigt T, Subramaniam K V, Shah S P. Nondestructive measurement of concrete strength gain by an ultrasonic wave reflection method. Materials and Structures, 2003, 36(262): 507–514
121. Voigt T, Akkaya Y, Shah S P. Determination of early age mortar and concrete strength by ultrasonic wave reflections. Journal of Materials in Civil Engineering, 2003, 15(3): 247–254
122. Demirboga R, Türkmen İ, Karakoc M B. Relationship between ultrasonic velocity and compressive strength for high-volume mineral-admixtured concrete. Cement and Concrete Research, 2004, 34(12): 2329–2336
123. Subramaniam K V, Mohsen J, Shaw C. Ultrasonic technique for monitoring concrete strength gain at early age. ACI Materials Journal, 2002, 99: 458–462
124. Wang D, Zhu H. Monitoring of the strength gain of concrete using embedded PZT impedance transducer. Construction & Building Materials, 2011, 25(9): 3703–3708
125. Gu H, Song G, Dhonde H, Mo Y L, Yan S. Concrete early-age strength monitoring using embedded piezoelectric transducers. Smart Materials and Structures, 2006, 15(6): 1837–1845
126. Cai D, Dai H, He X, Cai S, Zhang C. Application of fiber optical sensing technology to the Three Gorges Project. In: 4th International Conference of Dam Engineering, 2004, 147–154
127. Lin Y B, Chang K C, Chern J C, Wang L A. The health monitoring of a prestressed concrete beam by using fiber Bragg grating sensors. Smart Materials and Structures, 2004, 13)(4): 712–718
128. American society for testing and materials, ASTM C157 standard test method for length change of hardened hydraulic-cement mortar and concrete. Annual book of ASTM standards, Concrete and Concrete Aggregates. 1997, 04-02: 96–101
129. Yoo D Y, Park J J, Kim S W, Yoon Y S. Early age setting, shrinkage and tensile characteristics of ultra high performance fiber reinforced concrete. Construction & Building Materials, 2013, 41: 427–438
130. Yang Y, Sato R, Kawai K. Autogenous shrinkage of high-strength concrete containing silica fume under drying at early ages. Cement and Concrete Research, 2005, 35(3): 449–456
131. Yılmazturka F, Kulur S, Pekmezcia B Y. Measurement of shrinkage in concrete samples by using digital photogrammetric methods. International Archives of the Photogrammetry, Remote Sensing and Spatial Information Sciences, 2004, 34
132. Chen T, Yin W, Ifju P. Shrinkage measurement in concrete materials using cure reference method. Experimental Mechanics, 2010, 50(7): 999–1012
133. Newlands M, Paine K A, Vemuri N, Dhir R K. A linear test method for determining early-age shrinkage of concrete. Magazine of Concrete Research, 2008, 60(10): 747–757
134. ASTM C. 1581-04. Standard test method for determining age at cracking and induced tensile stress characteristics of mortar and concrete under restrained shrinkage, ASTM International, West Conshohocken, PA, 2004
135. Gesoglu M, Ozturan T, Güneyisi E. Effects of cold-bonded fly ash aggregate properties on the shrinkage cracking of lightweight concretes. Cement and Concrete Composites, 2006, 28(7): 598–605
136. Nazari A. Compressive strength of geopolymers produced by ordinary Portland cement: Application of genetic programming for design. Materials & Design, 2013, 43: 356–366
137. Sonebi M. Medium strength self-compacting concrete containing fly ash: Modelling using factorial experimental plans. Cement and Concrete Research, 2004, 34(7): 1199–1208
138. Siyal A A, Azizli K A, Man Z, Ullah H. Effects of parameters on the setting time of fly ash based geopolymers using Taguchi method. Procedia Engineering, 2016, 148: 302–307
139. Riahi S, Nazari A, Zaarei D, Khalaj G, Bohlooli H, Kaykha M M. Compressive strength of ash-based geopolymers at early ages designed by Taguchi method. Materials & Design, 2012, 37: 443–449